JOM 23478

Charge-transfer ion pairs with cationic bis(arene)iron(II) acceptors. Thermal electron-transfer catalysis of aromatic de-ligation *

J.K. Kochi and C.H. Wei

Chemistry Department, University of Houston, Houston, TX 77204-5641 (USA)

(Received September 14, 1992)

Abstract

Bis(hexamethylbenzene)iron dication $(HMB)_2Fe^{2+}$ forms a series of charge-transfer salts with anionic donors such as bromide, iodide, thiocyanate, tricyanomethide, tetraphenylborate and tetracarbonylcobaltate. X-Ray crystallography of the 1:2 tricyanomethide salt identifies the structural origin of the charge-transfer interaction for the contact ion pair, $[(HMB)_2Fe^{2+}, C(CN)_3^-]$. The strong carbonylmetalate donors $Co(CO)_4^-$ and $Mn(CO)_5^-$ promote the catalytic de-ligation of bis(arene)iron(II) by the electron-transfer chain (ETC) process previously identified in electrochemical and photochemical studies.

1. Introduction

Bis(arene)iron dications Ar_2Fe^{2+} with Ar = hexamethylbenzene, durene, mesitylene, etc. [1], can effectively serve as electron acceptors in the facile formation of weak charge-transfer complexes with neutral electron donors (D) such as ferrocene [2] and various aromatic hydrocarbons [3], *i.e.*

$$Ar_2Fe^{2+} + D \overset{K_{EDA}}{\rightleftharpoons} \underset{\text{(EDA complex)}}{[Ar_2Fe^{2+}, D]} \quad (1)$$

The formation of these electron donor-acceptor (EDA) complexes is detected by the spontaneous appearance of new visible absorption bands ($h\nu_{CT}$), which correlate linearly with the ionization potential of the donor (D) and the electron affinity of the acceptor (Ar_2Fe^{2+}), in accord with the Mulliken charge-transfer formulation [4,5].

The bis(arene)iron(II) acceptor is also highly susceptible to ion-pair formation in solution owing to the presence of the dipositive charge. Strong intermolecular (coulombic) interactions of oppositely charged ions can be considered in the generalized context of intimate or contact ion pairs (CIP) [6–8]. For example, characteristic charge-transfer absorption bands ($h\nu_{CT}$) have been identified in various N-substituted pyridinium salts that are constituted as electron acceptor/donor contact ion pairs, especially in nonaqueous solutions, *e.g.* [9,10]

$$XPy^+ + Co(CO)_4^- \rightleftharpoons \underset{\text{EDA (CIP)}}{[XPy^+, Co(CO)_4^-]} \xrightarrow{h\nu_{CT}} \text{etc.} \quad (2)$$

where X = alkyl, alkoxy, *etc.* [11].

In this study, we address the question as to how the sandwich-type structure of the cationic bis(arene)-iron(II) acceptor [12] affects the intermolecular charge-transfer interaction in the contact ion pair with various types of anionic donors (D^-), *i.e.*

(3)

Since a number of anions are also subject to ready oxidation [13], electron transfer within the contact ion pair in eqn. (3) will generate the metastable 19-e bis(arene)iron(I) monocation [14]. The novel catalytic consequences of such a redox process are also presented in detail.

Correspondence to: Professor J.K. Kochi.

* Dedicated to Professor Gian Paolo Chiusoli on the occasion of his retirement.

0022-328X/93/$6.00

2. Results

2.1. Charge-transfer spectra of bis(arene)iron(II) contact ion pairs

When a light orange solution of bis(hexamethylbenzene)iron(II) hexafluorophosphate $(HMB)_2Fe^{2+}(PF_6^-)_2$ in acetonitrile was mixed with the colorless tricyanomethide anion (as the potassium salt), the solution immediately took on the deep red coloration of the charge-transfer salt, *i.e.*

$$(HMB)_2Fe^{2+}(PF_6^-)_2 + 2\,K^+C(CN)_3^- \rightarrow \left[(HMB)_2Fe^{2+},\, 2\,C(CN)_3^-\right] + 2\,K^+PF_6^- \quad (4)$$

The quantitative effects of such a visual change were indicated in the electronic spectrum by the appearance of the new absorption band of $[(HMB)_2Fe^{2+}, C(CN)_3^-]$. Thus, Fig. 1 shows the results of the spectral (digital) subtraction of the $(HMB)_2Fe^{2+}$ component from the composite spectrum to expose the Gaussian envelope of the charge-transfer band with $\lambda_{max} = 464$ nm.

The charge-transfer absorption bands of $(HMB)_2Fe^{2+}$ with other anionic donors such as iodide, bromide, thiocyanate, tetraphenylborate and, tetracarbonylcobaltate were obtained by a similar procedure, and the values of λ_{CT} are listed in Table 1. For comparative purposes, Table 1 also includes the charge-transfer absorption bands of the planar cationic acceptor, 4-cyanopyridinium, with the same series of anionic donors encompassed by eqn. (2).

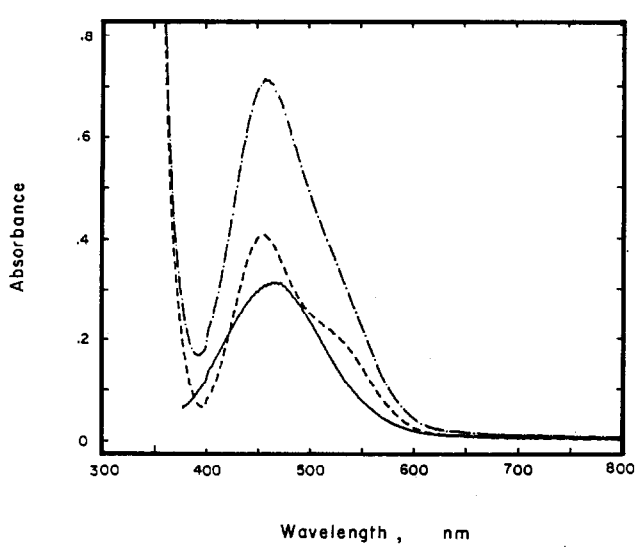

Fig. 1. Charge-transfer absorption band (———) obtained as a difference spectrum from the visible absorption (·–·–·) attendant upon the mixing of 0.005 M (HMB)$Fe(PF_6)_2$ (- - - - -) with 2 equiv. of $PPN^+C(CN)_3^-$ in acetonitrile at 23°C.

TABLE 1

Charge-transfer absorption spectra of the bis(HMB)iron(II) and 4-cyanopyridinium acceptors with various anionic donors [a]

Anionic donor	λ_{CT} [b,c] (nm)	λ_{CT} [b,d] (nm)
Bromide	387	339
Iodide	452 [e]	–
Thiocyanate	452	382
Tricyanomethide	464	383
Tetraphenylborate	357 [f]	~310
Tetracarbonylcobaltate	594 [e]	–

[a] In acetonitrile at 23°C. [b] λ_{max} of difference spectrum (see text), unless indicated otherwise. [c] $(HMB)_2Fe^{2+}$ acceptor. [d] 4-Cyanopyridinium acceptor. [e] Measured at −40°C. [f] Shoulder.

2.2. Isolation of crystalline charge-transfer salts of the bis(HMB)iron(II) acceptor

The charge-transfer salt of bis(hexamethylbenzene)iron(II) and tricyanomethide was isolated in essentially quantitative yields simply by the (*in vacuo*) concentration of the acetonitrile solution containing $(HMB)_2Fe^{2+}(PF_6^-)_2$ and slightly more than 2 equiv. of $K^+C(CN)_3^-$. The 1:2 stoichiometry for the cation/anion EDA pair (see eqn. (4)) was established by elemental analysis, as described in the Experimental section.

The charge-transfer salts of $(HMB)_2Fe^{2+}$ with bromide and tetraphenylborate were also isolated as orange crystals with 1:2 stoichiometry, by the metathesis of $(HMB)_2Fe^{2+}(PF_6^-)_2$ with tetra-n-butylammonium bromide and sodium tetraphenylborate, respectively, in acetonitrile solution at 23°C. However, when the same procedure was applied to $(HMB)_2Fe^{2+}$ and tetracarbonylcobaltate [as the bis(triphenylphosphoranylidene)ammonium or PPN salt], the purple CT absorption was transient and no bis(HMB)iron(II) salt could be isolated. Accordingly, the charge-transfer band of $[(HMB)_2Fe^{2+}, Co(CO)_4^-]$ as listed in Table 1 was obtained by mixing the (pre-cooled) component solutions at −40°C.

2.3. X-Ray crystallography of $[(HMB)_2Fe^{2+}, 2\,C(CN)_3^-]$

The single (dark red) crystal of $[(HMB)_2Fe^{2+}, 2\,C(CN)_3^-]$ suitable for X-ray crystallography was grown from a mixture of acetonitrile and diethyl ether in the monoclinic space group $P2_1/n$ with $a = 10.036(2)$ Å, $b = 10.597(3)$ Å, $c = 13.771(4)$ Å, $\beta = 92.45(2)°$ and $V = 1463$ Å^3. The diffraction data and the crystallographic processing parameters (see Experimental section) were treated by standard methods, and the ORTEP diagram of the charge-transfer salt is presented in Fig. 2. The cationic acceptor moiety $(HMB)_2Fe^{2+}$ consists of a pair of hexamethylbenzene rings locked in an eclipsed conformation about the iron center. The methyl groups are all slightly bent out of the benzene

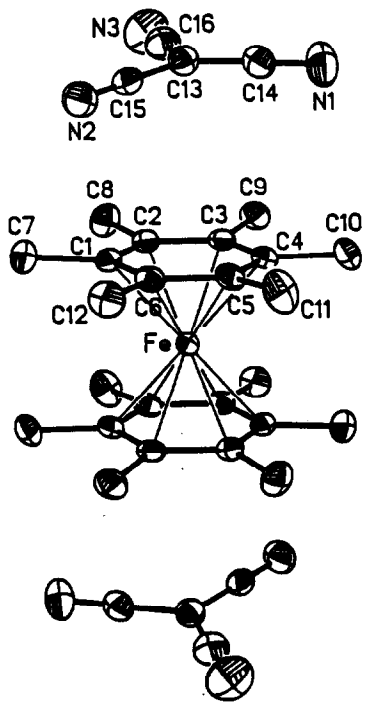

Fig. 2. ORTEP diagram of the charge-transfer salt $[(HMB)_2Fe^{2+}, 2\ C(CN)_3^-]$ with thermal ellipsoids as 40% equiprobability envelopes. Hydrogens are omitted for clarity.

plane, away from iron and the opposed methyl groups for minimal (non-bonded) steric interaction. The anionic donor moiety is not completely planar, $C(CN)_3^-$ showing a slight distortion towards a trigonal pyramidal configuration. Most importantly, the charge-transfer interaction in $[(HMB)_2Fe^{2+}, 2\ C(CN)_3^-]$ derives from a tricyanomethide donor lying on top of each HMB face, slightly displaced from the aromatic centroid and tilted at a 6° dihedral angle, at an average interionic separation of 3.45 Å. The stacking of the charge-transfer ion pairs in the crystal, as illustrated in Fig. 3, occurs with an average separation between adjacent anion planes of 3.80 Å.

2.4. *Ionic equilibria of bis(arene)iron(II) and tricyanomethide in solution*

Although the charge-transfer complexes of the dicationic bis(arene)iron(II) acceptor were consistently isolated as crystalline 1:2 salts, the ionic equilibria of the triple salt in solution must consist of contact ion pairs and contact ion triplets, *i.e.*

$$Ar_2Fe^{2+} + 2\ D^- \overset{K_1}{\rightleftharpoons} [Ar_2Fe^{2+}, D^-] + D^- \overset{K_2}{\rightleftharpoons} [Ar_2Fe^{2+}, 2\ D^-] \quad (5)$$

Careful examination of the difference (charge-transfer) spectra, obtained at the extremes of very high and low concentrations of $(HMB)_2Fe^{2+}$ relative to $C(CN)_3^-$, revealed no definitive spectral band shifts to distinguish the 1:1 and 1:2 EDA stoichiometries in eqn. (5) [15]. However, the linear change in the charge-transfer absorbance at $\lambda_{max} = 464$ nm with added tricyanomethide salt, as shown in Fig. 4, is consistent with the ionic equilibria in eqn. (5). Thus following Ebbesen and Ferraudi's study of (divalent) methylviologen or MV^{2+} complexes [16], we take the association constant K_1 to be significantly larger than K_2 in acetonitrile, *i.e.* the contact ion pair to be relatively insensitive to added donor [17]. The concentration dependence of the charge-transfer absorbance (A_{CT}) is then given by the Benesi–Hildebrand relationship [18]

$$\frac{[CIP]}{A_{CT}} = \frac{1}{\epsilon_{CT}} + \frac{1}{K_2\epsilon_{CT}}[C(CN)_3^-]^{-1} \quad (6)$$

where [CIP] is the concentration of the bis(arene) iron(II) acceptor, under conditions in which the tricyanomethide donor is present in excess. The formation constant and the extinction coefficient of the charge-transfer salt $[(HMB)_2Fe^{2+}, 2\ C(CN)_3^-]$ were

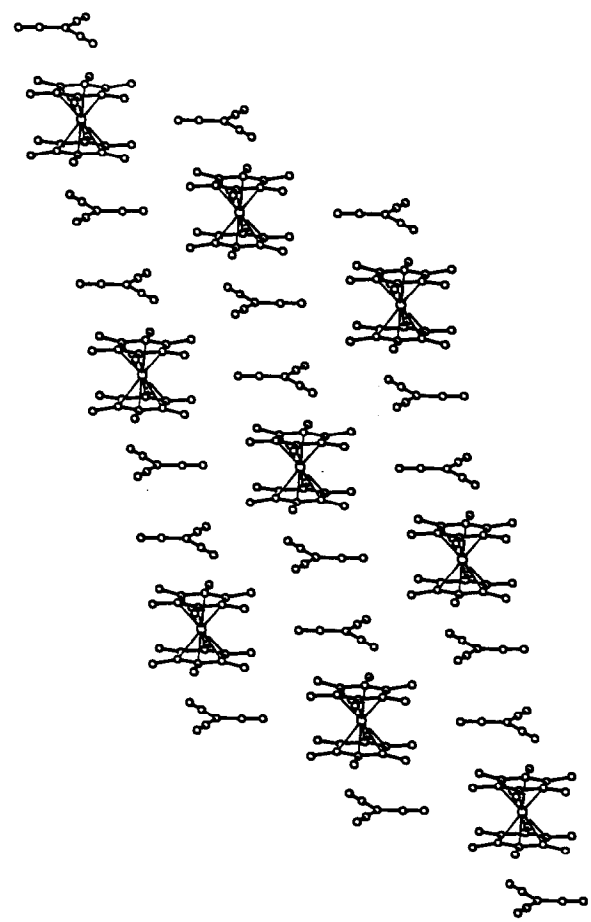

Fig. 3. Stacking of the $(HMB)_2Fe^{2+}$ and $C(CN)_3^-$ as acceptor/donor ion pairs in the *ab* plane.

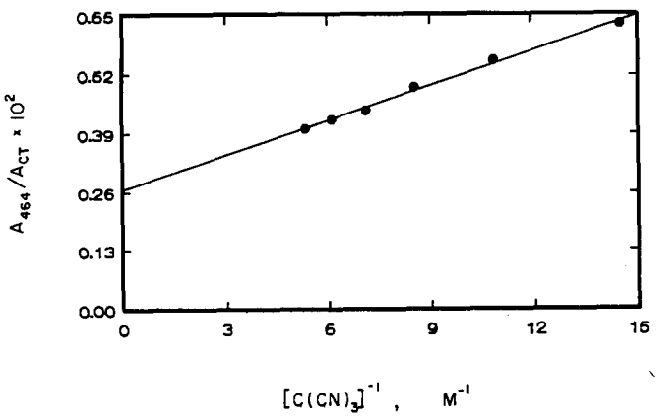

Fig. 4. Benesi–Hildebrand plot of the 464-nm charge-transfer absorbance for $[(HMB)_2Fe^{2+}, C(CN)_3^-]$ with the variation of $[C(CN)_3^-]^{-1}$ in acetonitrile at 23°C.

evaluated from the slope and intercept in Fig. 4 as $K_2 = 0.01\ M^{-1}$ and $\epsilon_{CT} = 380\ M^{-1}\ cm^{-1}$, respectively [19]. From the measurement of the charge-transfer absorbance at low concentrations of tricyanomethide relative to bis(HMB)iron(II), the extinction coefficient of the contact ion pair $[(HMB)_2Fe^{2+}, C(CN)_3^-]$ was estimated as $\epsilon_{CIP} \sim 150\ M^{-1}\ cm^{-1}$, or roughly half that of the contact ion triplet.

The medium effect on the charge-transfer salt was limited to rather polar solvents such as acetone and acetonitrile, owing to its insolubility in dichloromethane and benzene. The slight bathochromic shift of the absorption band to lower energies, as well as the hypochromic diminution of the charge-transfer absorbance, with decreasing solvent polarity in Fig. 5(A) is consistent with the strong ground-state stabilization extant in the contact ion pair. Such a minor perturbation of bis(HMB)iron(II) salts contrasts strongly with the large solvent effect previously observed in uni-/univalent charge-transfer salts [10].

Addition of small amounts of the redox-inert salt tetra n-butylammonium hexafluorophosphate (TBAH) to the acetonitrile solution of $[(HMB)_2Fe^{2+}, 2\ C(CN)_3^-]$ induced the large hypochromic change shown in Fig. 5(B). Indeed the monotonic decrease in the charge-transfer absorbance with increasing amounts of added TBAH was characteristic of the facile competition for the contact ion pair, *e.g.*

$$(HMB)_2Fe^{2+}C(CN)_3^- + Bu_4N^+PF_6^- \overset{K_x}{\rightleftharpoons} (HMB)_2Fe^{2+}PF_6^- + Bu_4N^+C(CN)_3^- \quad (7)$$

The direct relationship between the charge-transfer absorbance and added TBAH, as modulated by the simple ion-pair equilibrium in eqn. (7) could not be developed in a quantitative manner [11] owing to complications from the (additional) ionic exchange with the contact ion triplet (see eqn. (5)) [19].

2.5. *Electron-transfer catalysis of bis(HMB)iron(II) by carbonylmetallate donors*

The charge-transfer absorption band of the bis-(HMB)iron(II) acceptor and the tetracarbonylcobaltate donor, as listed in Table 1, could only be observed (transiently) at −40°C owing to competition from a facile thermal process. The latter occurred so rapidly with the analogous pentacarbonylmanganate donor that the charge-transfer band of the $(HMB)_2Fe^{2+}$ complex could not be reliably measured. A rapid thermal reaction also accompanied the treatment of other bis-

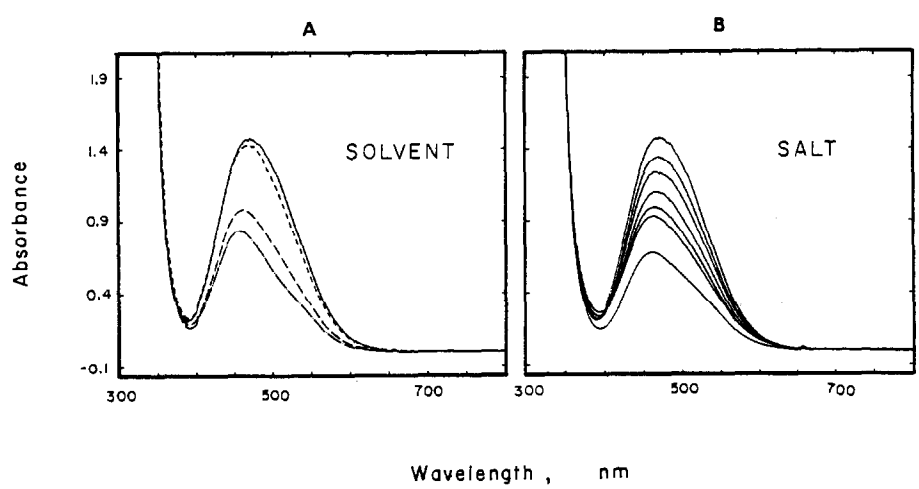

Fig. 5. Solvent (A) and salt (B) effects on the charge-transfer absorbance from 0.005 M $(HMB)_2Fe^{2+}$ and 0.005 M $C(CN)_3^-$ at 23°C. Left (top-to-bottom): THF/CH_3CN (1:1, v/v), acetone, THF/CH_3CN (1:3, v/v) and CH_3CN. Right (top-to-bottom): 0, 0.5, 1.0, 2.0, 3.0, 4.0, and 8.0 equiv. of added tetrabutylammonium hexafluorophosphate to THF/CH_3CN (1:1, v/v).

(arene)iron(II) acceptors, such as those containing mesitylene (MES) and durene (DUR) ligands, with even weak anionic donors such as bromide and tricyanomethide. Thus the importance of these thermal processes generally followed the increasing trend in the reduction potentials (E^0_{red}) of the bis(arene)iron(II) acceptors in the order [20]: $(MES)_2Fe^{2+} > (DUR)_2Fe^{2+} > (HMB)_2Fe^{2+}$ and the decreasing oxidation potentials (E^0_{ox}) of the anionic donors in the order [21]: $Br^- < C(CN)_3^- < Co(CO)_4^- < Mn(CO)_5^-$.

The thermal reaction between $(HMB)_2Fe^{2+}$ and $Co(CO)_4^-$ was accompanied by a dramatic change in the acetonitrile solution (immediately upon mixing) from orange to purple, which persisted for a while and then faded to a pale lime color, all occurring within a period of ~ 15 min at 23°C. Spectral examination of the transient purple solution revealed the presence of a new absorption band at $\lambda_{max} = 582$ nm, which corresponded to that of the monocation bis(HMB)iron(I) (λ_{max} 580 nm, ϵ_{max} 604 M^{-1} cm^{-1} in acetone) [14]. For confirmation, an authentic sample of the latter was independently prepared as the hexafluorophosphate salt by spontaneous crystallization from aqueous solution during the dithionite reduction of $(HMB)_2Fe^{2+}(PF_6^-)_2$ according to Anderson and Drago [22]. The series of time-resolved spectra in Fig. 6(A) show the typical transitory behavior of the monocation $(HMB)_2Fe^+$ as a metastable intermediate in solution, initially emerging out of the reduction of $(HMB)_2Fe^{2+}$ (λ_{max} 450 nm), with its concentration reaching a plateau, and then disappearing completely (as shown by the spectral decay back to the baseline). The analogous spectral changes accompanying the thermal reaction of $(HMB)_2Fe^{2+}$ and $Mn(CO)_5^-$ in Fig. 6(B) emphasize the (essentially) instantaneous reduction of the dicationic bis(HMB)iron(II) acceptor by this strong anionic donor. The spectral changes in Figs. 6(A) and (B), despite their appearances, are indeed equivalent if the relative differences in the 450 and 582 nm absorbances of $(HMB)_2Fe^{2+}$ and $(HMB)_2Fe^+$, respectively, are merely recognized.

Quantitative ^1H NMR analysis of the bleached solution indicated that the proton resonance of bis(HMB)iron(II) is completely replaced by that of the free ligand; and the presence of 2 equiv. of hexamethylbenzene in solution was confirmed by gas chromatographic analysis using the internal standard method. Coupled with the iron analysis carried out with 2,2'-bipyridine (bpy) and the spectrophotometric determination of $Fe(bpy)_3^{2+}$ at $\lambda = 520$ nm ($\epsilon = 7994$ M^{-1} cm^{-1}) [23], the stoichiometry of the thermal reaction was established as

$$(HMB)_2Fe^{2+} \xrightarrow[CH_3CN]{[Co(CO)_4^-]} 2\ HMB + Fe(NCCH_3)_6^{2+} \quad (8)$$

The catalytic nature of the transformation in eqn. (8) was demonstrated by infrared analysis of the reaction mixture, which showed that the tetracarbonylcobaltate donor was intact, the absorbance of the carbonyl stretching band at $\nu(CO) = 1892$ cm^{-1} being essentially (±3%) undiminished. Furthermore, the same analytical results were obtained from the thermal reaction of $(HMB)_2Fe^{2+}$ with pentacarbonylmanganate. It is noteworthy that in those reactions carried out with excess (2 equiv.) $Mn(CO)_5^-$, a small amount (< 3%) of dimanganese decarbonyl could be detected by its characteristic IR bands at $\nu(CO) = 2045$, 2009 and 1980 cm^{-1} [24]. Since such a dimeric carbonylmetal byproduct is symptomatic of a redox change [25], the transformation in eqn. (8) is hereafter designated

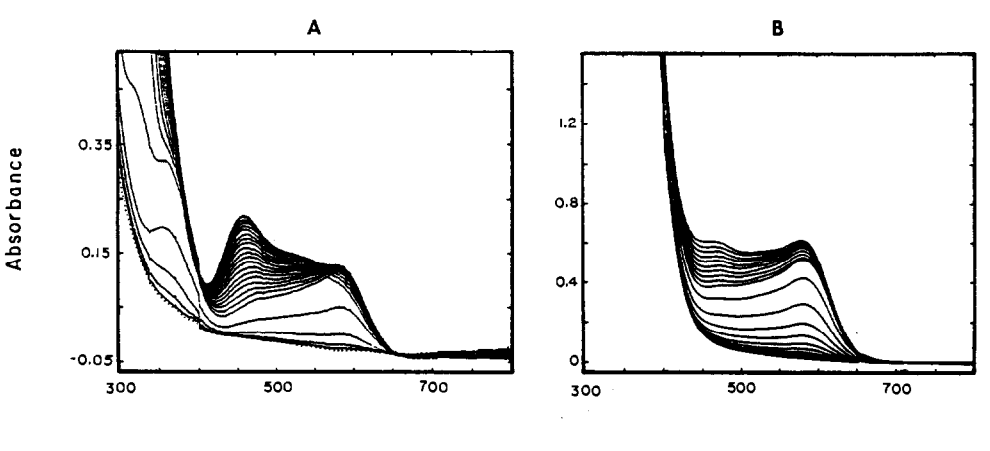

Fig. 6. Spectral changes accompanying the catalytic de-ligation of 0.003 M $(HMB)_2Fe^{2+}$ with (A) 0.1 equiv. of $PPN^+Co(CO)_4^-$ and (B) 0.3 equiv. of $PPN^+Mn(CO)_5^-$ in acetonitrile.

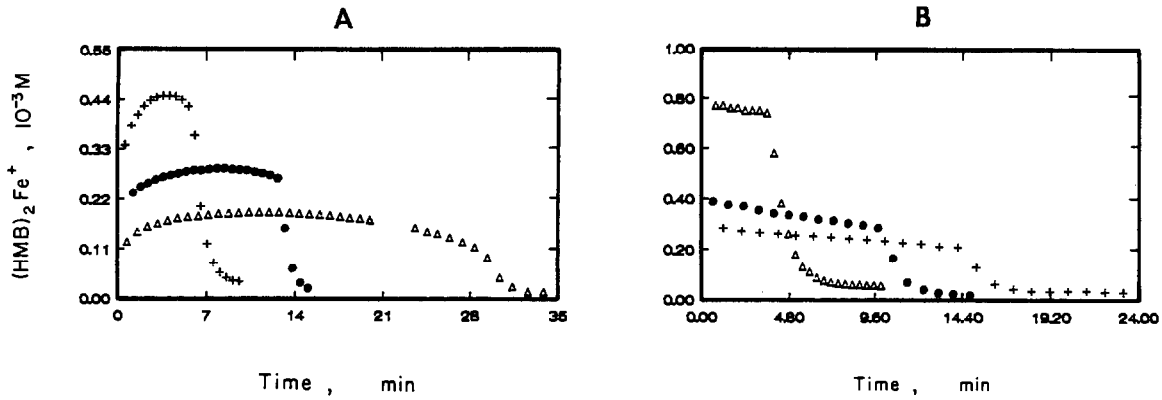

Fig. 7. Rate profile for the catalytic de-ligation of 0.003 M $(HMB)_2Fe^{2+}$ with 5, 10 and 30% (bottom-to-top) of added $Co(CO)_4^-$ (A) and $Mn(CO)_5^-$ (B) in acetonitrile by monitoring the concentration of $(HMB)_2Fe^+$ at $\lambda_{max} = 582$ nm.

as electron-transfer catalysis of bis(arene)iron(II) de-ligation.

2.6. *Distinctive rate profiles for bis(HMB)iron(II) de-ligation*

The course of bis(HMB)iron(II) de-ligation according to eqn. (8) was spectrally monitored by following the change in the 582-nm absorbance of $(HMB)_2Fe^+$ in acetonitrile at 23°C. The results in Fig. 7(A) typically show the rate profiles to consist of three distinct phases consisting of (a) the rise, (b) the plateau, and (c) the fall in concentration of the $(HMB)_2Fe^+$ transient at three concentrations of $Co(CO)_4^-$ representing relatively low, intermediate, and high levels of anionic donor. Clearly, the steady-state concentration of the transient increased with $[Co(CO)_4^-]$, but at the expense of the duration of the catalytic chain. The same relationship also held for the catalysis by $Mn(CO)_5^-$, as shown in Fig. 7(B); but the rate profile for this anionic donor showed no initial phase (a) arising from the prior reduction of bis(HMB)iron(II). On the other hand, as the level of the cationic acceptor was increased relative to $[Mn(CO)_5^-]$, the duration of the catalytic chain was relatively unaffected, despite the (expected) increase in the steady-state concentration of the $(HMB)_2Fe^+$ transient, as shown in Fig. 8.

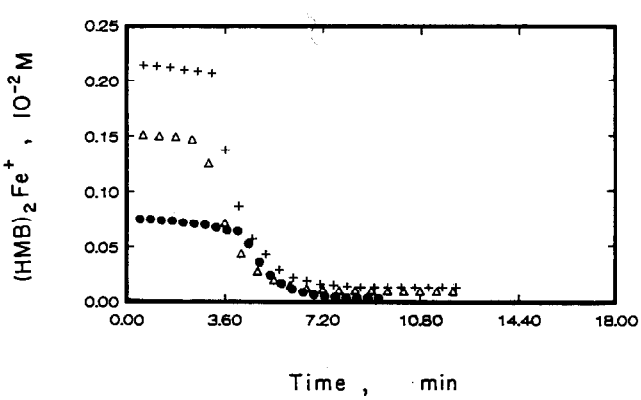

Fig. 8. Effect of acceptor concentration on the catalytic de-ligation of (bottom-to-top) 0.0030, 0.0045 and 0.0060 M $(HMB)_2Fe^{2+}$ and 0.0003 M $PPN^+Mn(CO)_5^-$ in acetonitrile at 23°C, as in Fig. 7.

3. Discussion

The bis(arene)iron(II) complex by virtue of its dipositive charge is an effective electron acceptor for various anionic donors, including bromide, thiocyanate, tricyanomethide, and tetraphenylborate. The extensive formation of contact ion pairs, even in polar (aprotic) solvents such as acetonitrile, is indicated by the ubiquitous presence of charge-transfer absorption bands of the type previously observed with the (uni-/univalent) pyridinium salts only in nonpolar solvents [10]. In such contact ion pairs, the charge-transfer transition can be generally approximated as [13]

$$h\nu_{CT} \simeq E^0_{ox}(D^-) + E^0_{red}(A^+) + \text{constant} \qquad (9)$$

where E^0_{ox} is the oxidation potential of the anionic donor and E^0_{red} is the reduction potential of the cationic acceptor. The X-ray crystallographic structure shown by the ORTEP diagram in Fig. 2 establishes the relevant charge-transfer interaction in the contact ion pair to derive from the contiguous placement of the anionic (tricyanomethide) donor cofacial to the arene (HMB) ligand of the cationic acceptor. Accordingly, the potential difference $(E^0_{ox} + E^0_{red})$ in eqn. (9) represents the HOMO–LUMO gap of the charged donor/acceptor pair $[D^-, Ar_2Fe^{2+}]$ [13]. As applied to the charge-transfer absorption bands of the series of bis(HMB)iron(II) complexes in Table 1, the value of E^0_{red} is constant, and eqn. (9) predicts the decreasing (less positive) oxidation potentials of the anionic donors in the order: $BPh_4^- > Br^- > I^- \approx SCN^- > C(CN)_3^- \gg$

$Co(CO)_4^-$ to parallel the increasing trend of λ_{CT}. Quantitative measures of the donor strengths of anions are otherwise unavailable from transient electrochemical techniques [26], owing to the irreversible nature of the oxidation step ($D^- \rightarrow D + e$) for most of these redox pairs [13].

The identification of the organometallic carbonylmetalate anions $Co(CO)_4^-$ and $Mn(CO)_5^-$ as particularly effective electron donors can also be deduced from their role in the efficient catalytic chain process for arene de-ligation according to eqn. (8). Thus the previous electrochemical study identified the reduced acceptor, *i.e.*, $(HMB)_2Fe^+$, as the reactive intermediate responsible for the rapid de-ligation via an electron-transfer chain (ETC) process [20], as shown in Scheme 1, where the subscript s denotes (acetonitrile) solvation.

$$(HMB)_2Fe^+ \xrightarrow{k_2} 2\ HMB + Fe_s^+ \qquad (10)$$

$$Fe_s^+ + (HMB)_2Fe^{2+} \underset{k_{-3}}{\overset{k_3}{\rightleftharpoons}} Fe_s^{2+} + (HMB)_2Fe^+, \textit{ etc.} \qquad (11)$$

Scheme 1.

In the electron-transfer catalysis of arene de-ligation (eqn. (8)), the propagation steps as outlined in Scheme 1 are preceded by an initiation step which involves the prior reduction (k_1) of the bis(arene)iron(II) acceptor, *i.e.*

$$(HMB)_2Fe^{2+} + M(CO)_n^- \underset{k_{-1}}{\overset{k_1}{\rightleftharpoons}} M(CO)_n^{\cdot} + (HMB)_2Fe^+ \qquad (12)$$

where $M(CO)_n^-$ is either $Co(CO)_4^-$ or $Mn(CO)_5^-$. The co-generation of the 17-e carbonylmetal radical in eqn. (12) then provides the means for chain termination *via* the interception of the chain-carrying iron species.

$$M(CO)_n^{\cdot} + Fe_s^+ \xrightarrow{k_4} Fe_s^{2+} + M(CO)_n^- \qquad (13)$$

or dimerization

$$2\ M(CO)_n^{\cdot} \xrightarrow{k_5} M_2(CO)_{2n} \qquad (14)$$

The long catalytic chain lengths observed in arene de-ligation indicates that the carbonylmetal radicals are efficiently intercepted in eqn. (13) relative to their bimolecular coupling in eqn. (14). (Note the low yields of $Mn_2(CO)_{10}$ detected in the carbonylmanganate-induced de-ligation of $(HMB)_2Fe^{2+}$; the analogous $Co_2(CO)_8$ is not observed owing to its rapid disproportionation in acetonitrile [27].)

In order to test the validity of the ETC mechanism for the catalytic de-ligation of $(HMB)_2Fe^{2+}$, the differential rate equations relating to eqns. (10)–(14) can be numerically integrated with the aid of the iterator computer program GIT developed by Weigert [28] based on the algorithms by Gear [29]. Owing to the distinctive rate profiles observed in Figs. 6–8, the computer simulations focus on the concentration changes of the reactive intermediate $(HMB)_2Fe^+$. Each of the five independent parameters is individually optimized, as described in the Experimental section. The graphical fits to the rate profiles are found to be most sensitive to the initiation rate (k_1) and the propagation rate (k_2), as given by eqns. (12) and (10), respectively. Back electron transfer (k_{-1}) in the initiation step is dependent on the redox equilibrium with $k_1/k_{-1} = \Delta E_1/RT$, where the driving force ΔE_1 is separately

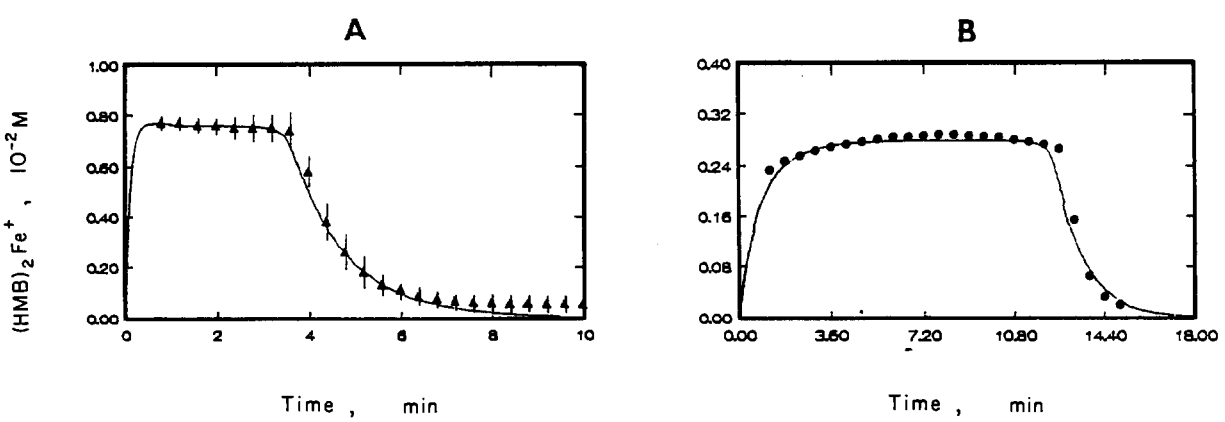

Fig. 9. Computer simulation (smooth curve) of the rate profiles for catalytic de-ligation with the aid of the Gear Iterator [28] for the experimental rate profiles from 0.003 M $(HMB)_2Fe^{2+}$ and (A) 0.3 equiv. of $Mn(CO)_5^-$ (▲) and (B) 0.1 equiv. of $Co(CO)_4^-$ (●) using the rate constants for eqns. (10)–(14), as given in the text.

determined from E^0_{ox} of $M(CO)^-_n$ and E^0_{red} of $(HMB)_2Fe^{2+}$ evaluated earlier [20,30]. Analogously, the back electron transfer (k_{-3}) in the propagation step is dependent on $k_3/k_{-3} = \Delta E_3/RT$ with E^0_{ox} of Fe^+_s obtained from an earlier measurement [31].

For the catalytic de-ligation induced by $Mn(CO)^-_5$, the graphical fit of the calculated curve to the experimental points as shown in Fig. 9(A) is based on the optimized parameters $k_1 = 61\ M^{-1}\ s^{-1}$, $k_2 = 1.4 \times 10^{-2}\ s^{-1}$, $k_3 = 3.6 \times 10^3\ M^{-1}\ s^{-1}$, $k_5 = 7.0 \times 10^8\ M^{-1}\ s^{-1}$ with $k_{-1}/k_1 = 110$. The cross termination rate constant $k_4 = 2 \times 10^{10}\ M^{-1}\ s^{-1}$ is diffusion controlled (and it is verified by initially setting k_5 and then optimizing k_4). Further support for this kinetics model is provided by the optimized termination rate constant k_5 for the HOMO coupling of $Mn(CO)^0_5$, which is consistent with the independently reported value ($9.5 \times 10^8\ M^{-1}\ s^{-1}$) in hexane solution [32]. Most importantly, the oxidation potential of $E^0_{ox} = -0.14$ V for $Mn(CO)^-_5$ that is predicted (from the optimized value of k_{-1}/k_1 and $E^0_{red} = -0.26$ V *vs.* SCE for $(HMB)_2Fe^{2+}$) is in agreement with an earlier measurement (-0.142 V) by Tilset and Parker [30].

The catalytic de-ligation of $(HMB)_2Fe^{2+}$ by $Co(CO)^-_4$ can also be evaluated by the same iterative procedure. The graphical fit shown in Fig. 9(B) was obtained with the optimized parameters $k_1 = 7.4\ M^{-1}\ s^{-1}$, $k_{-1} = 4.7 \times 10^7\ M^{-1}\ s^{-1}$, $k_2 = 1.4 \times 10^{-2}\ s^{-1}$, and $k_3 = 4.0 \times 10^3\ M^{-1}\ s^{-1}$. The termination rate constant $k_5 = 4.0 \times 10^8\ M^{-1}\ s^{-1}$ was taken from an earlier study by Wegman and Brown [33], and an additional termination rate constant $k_6 = 3.3 \times 10^5\ M^{-1}\ s^{-1}$ was necessary (see Experimental section). It is noteworthy that $E^0_{ox} = 0.14$ V (that is evaluated from the optimized redox equilibrium $k_{-1}/k_1 = 1.6 \times 10^7$ and E^0_{red} of $(HMB)_2Fe^{2+}$) is in good agreement with the reversible potential of 0.135 V determined electrochemically [20].

Confidence in the curve-fitting procedure for the ETC mechanism of catalytic de-ligation, as described by eqns. (10)–(14), is provided by the agreement in the propagation rate constants $k_2 = 1.4 \times 10^{-2}\ s^{-1}$ and $k_3 = 3.8 \pm 0.2 \times 10^3\ M^{-1}\ s^{-1}$ obtained from the two different systems. Furthermore, the optimized value of k_3 from the simulation accords with the rate constant of $4 \times 10^3\ M^{-1}\ s^{-1}$ estimated from the Marcus relationship using the value of $E^0_{ox} = -0.9$ V *vs.* Cp_2Fe for Fe^+_s obtained from the earlier pulse voltammetric study [31]. However, the de-ligation rate constant is about an order of magnitude slower than that evaluated by cyclic voltammetry in the presence of added (0.1 M) tetra-n-butylammonium hexafluorophosphate as the supporting electrolyte [20]. Thus the most important kinetic factor that distinguishes the rate profiles for catalytic de-ligation induced by $Mn(CO)^-_5$ from that by $Co(CO)^-_4$, as shown in Fig. 7, is the initiation rate constant (k_1). The rate factor of ~ 10, which favors $Mn(CO)^-_5$ over $Co(CO)^-_4$ is associated with the increased driving force for reduction (eqn. (12)) due to a more negative value of E^0_{ox}. Although this property also affects the termination rates, the visible effects on the rate profile (particularly in the final phases) are less obvious. The catalytic de-ligation of bis(arene)-iron(II) that is spontaneously induced by $Mn(CO)^-_5$ and $Co(CO)^-_4$ thus forms the thermal counterpart to the electrochemical [20] and photochemical [3] processes previously identified for ETC catalysis.

4. Experimental section

4.1. Materials

Bis(hexamethylbenzene)iron(II) hexafluorophosphate $(HMB)_2Fe^{2+}(PF^-_6)_2$ was prepared from anhydrous ferric chloride (Pennwalt), aluminum chloride (Fluka) and hexamethylbenzene (Aldrich) according to the literature procedure [34]. Bis(hexamethylbenzene) iron(I) hexafluorophosphate $(HMB)_2Fe^+PF^-_6$ was prepared by aqueous dithionite reduction of the iron(II) salt as described by Anderson and Drago [22]. Potassium tricyanomethide $KC(CN)_3$ was prepared from cyanoform [35], and converted to the PPN salt by metathesis with PPN^+Cl^- (Alfa) in water. The thiocyanate salt PPN^+SCN^- was similarly prepared from $NH^+_4SCN^-$. Tetra-n-butylammonium bromide, sodium tetraphenylborate and tetrabutylammonium hexafluorophosphate were commercial samples (Alfa), and used as received. The carbonylmetalate salts were prepared from $NaCo(CO)_4$ and $NaMn(CO)_5$ (as 0.1 M aqueous solutions) by treatment with an equimolar amount of PPN^+Cl^- under anaerobic conditions described earlier [35].

Acetonitrile (Mallinckrodt reagent) was stirred with 1% $KMnO_4$ for 24 h, and then heated under reflux for an additional hour. The mixture was filtered, and then successively redistilled from P_2O_5 and CaH_2 under an argon atmosphere. Tetrahydrofuran (Fisher reagent) was distilled from sodiobenzophenone and stored in a Schlenk flask under an argon atmosphere.

4.2. Instrumentation

UV-vis spectra were recorded on a Hewlett Packard 3450A diode array spectrometer with 2-nm resolution. ^1H NMR spectra were obtained on a JEOL FX90Q spectrometer, and the chemical shifts are reported in ppm relative to an internal TMS standard. Infrared spectra were recorded on a Nicolet 10DX FT-IR spectrometer using a 1.0 mm NaCl cell (solution), Nujol mull or KBr disc.

4.3. Synthesis of bis(hexamethylbenzene)iron(II) charge-transfer salts

4.3.1. Tricyanomethide salt

A solution of $KC(CN)_3$ (0.054 g, 0.42 mmol) in 5 ml of water was added to a stirred solution of 0.10 g of $(HMB)_2Fe(PF_6)_2$ in 5 ml of acetone. The resulting solution was concentrated *in vacuo*. The red residue was washed with water, and recrystallized from a mixture of acetonitrile and ether to yield red crystals of $(HMB)_2Fe[C(CN)_3]_2$ in essentially quantitative yields. Anal. Found [37]: C, 68.34; H, 6.48; N, 15.08. $C_{32}H_{36}N_6Fe$ calcd.: C, 68.56; H, 6.47; N, 15.00%. IR (KBr): ν(CN) 2165 cm^{-1}. ^1H NMR (CD_3CN): 2.26 (methyl).

4.3.2. Bromide salt

A solution of tetra-n-butylammonium bromide (0.11 g, 0.34 mmol) in 5 ml of acetonitrile was added to a stirred solution of 0.10 g (0.015 mmol) of $(HMB)_2Fe(PF_6)_2$ in 5 ml of acetonitrile. The orange solid was collected, washed with acetonitrile and recrystallized from 10% by vol. aqueous acetonitrile of $(HMB)_2FeBr_2 \cdot 3H_2O$. Anal. Found [37]: C, 48.23; H, 7.12. $C_{24}H_{42}Br_2O_3Fe$ calcd.: C, 48.51; H, 7.12%.

4.3.3. Tetraphenylborate salt

A solution of 0.11 g (0.32 mmol) of $NaBPh_4$ in 5 ml of acetonitrile was added to a stirred solution of 0.10 g (0.15 mmol) of $(HMB)_2Fe(PF_6)_2$ in 5 ml of acetonitrile. The orange solid was collected and successively washed with water, acetonitrile and diethyl ether to afford $(HMB)_2Fe(BPh_4)_2$ in ~95% yield. Anal. Found [37]: C, 84.99; H, 7.57. $C_{72}H_{76}B_2Fe$ calcd.: C, 84.88; H, 7.52%.

4.4. Catalytic de-ligation of bis(HMB)iron(II) with carbonylmetalates

In a typical procedure, a mixture of 8.6 mg (0.012 mmol) of $PPN^+Co(CO)_4^-$ and 2.7 mg (0.0040 mmol) of $(HMB)_2Fe(PF_6)_2$ was treated in 2 ml of acetonitrile. Upon mixing, the solution immediately became brown and then purple. The purple solution persisted for a few minutes and gradually faded to a distinctive lime color. Quantitative IR analysis of the reaction mixture indicated that 95% of $Co(CO)_4^-$ was retained in solution, as judged by its carbonyl stretching band at ν(CO) = 1892 cm^{-1}. A measured aliquot of the solution was diluted with water, and excess 2,2'-bipyridine (bpy) was added. A total of 4.0 μmol of $Fe(bpy)_3^{2+}$ was determined spectrophotometrically by its distinctive band λ_{max} = 520 nm with ϵ_{max} = 7994 M^{-1} cm^{-1} in aqueous acetonitrile [3]. When the thermal reaction was carried out in acetonitrile-d_3, 2.0 equiv. of hexamethylbenzene (relative to iron) was detected by ^1H NMR spectrophotometry using nitromethane as the internal standard. Essentially the same results were obtained when $PPN^+Mn(CO)_5^-$ was used as the carbonylmetalate initiator.

For the kinetics study, a 0.30 mM solution of $(HMB)_2Fe(PF_6)_2$ in acetonitrile was added to calculated amounts (either 5, 10 or 30%) of $PPN^+Co(CO)_4^-$ dissolved in a very small amount of tetrahydrofuran. The course of the thermal reaction was monitored by following the absorbance decrease in the visible absorption band with λ_{max} 582 nm. The same procedure was used for $(HMB)_2Fe(PF_6)_2$ and $PPN^+Mn(CO)_5^-$.

The graphical simulation of the rate profiles shown in Fig. 9 was carried out with the aid of the Gear Iterator program [38] on an AT & T microcomputer. In the simulation of the $Mn(CO)_5^-$ curves, the systematic variation of the rate constants for eqns. (10)–(14) led to values of k_1 and k_2 in the range 57–64 M^{-1} s^{-1} and $(1.3–1.5) \times 10^{-2}$ s^{-1}, respectively. The simulations were rather insensitive to the values of k_3, k_4 and k_5 in the range $8 \times 10^2–2 \times 10^4$ M^{-1} s^{-1}, 2×10^{10} M^{-1} s^{-1}, and 7×10^8 M^{-1} s^{-1}, respectively. The highly exergonic driving force for electron-transfer in the termination step (eqn. (13)), essentially precludes back electron transfer. Reversible electron transfer in the initiation step (eqn. (12)) was optimized as k_{-1}/k_1 in the region 90–180. Essentially the same procedure was used for the simulation of the $Co(CO)_4^-$ curves. The value of k_1 was optimized in the range 6–8 M^{-1} s^{-1}, and $k_{-1} < 3 \times 10^8$ M^{-1} s^{-1}. In addition to the usual optimization of k_2, k_3 and k_4, an additional termination rate constant k_6 was necessitated for an optimum fit [39]. No dimeric $Co_2(CO)_8$ were detected upon the direct IR analysis of the reaction mixture.

4.5. Electronic spectra of charge-transfer salts

Spectroscopic measurements were all carried out under an atmosphere of argon in a 1.0-cm quartz cuvette equipped with Teflon valves. Solvent and salts effects on the electronic spectra in Fig. 5 were determined by the procedure described previously [10]. Due to the unstable nature of $(HMB)_2FePF_6$, the spectral measurements were carried out at 0°C by rapid manipulation of the solutions. The determination of the formation constants according to the Benesi–Hildebrand method was carried out as described earlier [36].

4.6. X-Ray crystallography of the bis(HMB)$_2$Fe$^+$-[C(CN)$_3^-$]$_2$ charge-transfer salt

A bright red prismatic block having approximate dimensions $0.48 \times 0.38 \times 0.18$ mm^3 was mounted in a random orientation on a Nicolet R3m/V automatic

diffractometer under a stream of dry nitrogen maintained at −50°C in order to retard decomposition. The radiation used was Mo $K\alpha$ monochromatized by a highly ordered graphite crystal. Final cell constants, as well as other information pertinent to data collection and refinement were $a = 10.036(2)$ Å, $b = 10.597(3)$ Å, $c = 13.771(4)$ Å, $\beta = 92.45(2)°$, $V = 1463$ Å^3, $Z = 2$, independent data with $I > 3\sigma(I) = 1943$, $R = 3.6\%$, $R_w = 3.6\%$ for $w = \sigma(F)^{-2}$. The Laue symmetry was determined to be $2/m$, and from the systematic absences noted the space group was shown unambiguously to be $P2_1/n$. Intensities were measured using the omega scan technique, with the scan rate depending on the count obtained in rapid pre-scans of each reflection. Two standard reflections were monitored every 2 h or every 100 data collected, and these showed no significant change. During data reduction, Lorentz and polarization corrections were applied; however, no correction for absorption was made due to the very small absorption coefficient. Since the asymmetric unit consisted of one-half dication and one anion, the structure was solved by simply positioning the Fe atom on an inversion center. The remaining non-hydrogen atoms were located in subsequent difference Fourier syntheses. The usual sequence of isotropic and anisotropic refinement was followed, after which all hydrogens were entered in ideal calculated positions and constrained to a riding motion. Eventually each of the methyl groups was treated as an ideal rigid body and allowed to rotate independently. After all shift/e.s.d. ratios were less than 0.1, convergence was reached at the agreement factors listed above (Table 2). No unusually high correlations were noted between any of the variables in the last cycle of full-matrix least squares refinement, and the final difference density map showed a maximum peak of about 0.2 e Å^{-3}. All calculations were made using Nicolet's SHELXTL PLUS (1987) series of crystallographic programs.

TABLE 2

Atomic coordinates ($\times 10^4$) and equivalent isotropic displacement parameters (Å$\times 10^3$) for [$(HMB)_2Fe^{2+}$, 2 $C(CN)_3^-$]

	x	y	z	U_{eq} [a]
Fe	5000	5000	5000	23(1)
N(1)	2422(3)	9455(3)	3554(2)	65(1)
N(2)	3336(3)	9067(3)	6712(2)	58(1)
N(3)	−476(3)	7605(4)	5437(3)	79(1)
C(1)	4157(3)	6135(3)	6123(2)	29(1)
C(2)	3111(3)	5657(3)	5503(2)	29(1)
C(3)	3145(3)	5843(3)	4472(2)	30(1)
C(4)	4227(3)	6501(3)	4074(2)	31(1)
C(5)	5265(3)	6993(3)	4705(2)	32(1)
C(6)	5240(3)	6797(3)	5724(2)	29(1)
C(7)	4099(3)	6021(3)	7220(2)	42(1)
C(8)	1923(3)	4999(4)	5916(2)	46(1)
C(9)	1967(3)	5405(3)	3826(2)	42(1)
C(10)	4264(3)	6747(3)	2992(2)	43(1)
C(11)	6351(3)	7793(3)	4272(3)	52(1)
C(12)	6325(3)	7353(3)	6398(2)	42(1)
C(13)	1723(3)	8762(3)	5235(2)	40(1)
C(14)	2105(3)	9157(3)	4313(3)	43(1)
C(15)	2604(3)	8932(3)	6052(2)	40(1)
C(16)	506(4)	8142(3)	5344(3)	51(1)

[a] Equivalent isotropic U defined as one-third of the trace of the orthogonalized U_{ij} tensor.

Acknowledgment

We thank J.D. Korp for crystallographic assistance, the National Science Foundation, Robert A. Welch Foundation, and the Texas Advanced Research Project for financial support.

References

1 (a) E. O. Fischer and R. Bottcher, *Chem. Ber., 89* (1956) 2937; (b) T. S. Cameron, M. D. Clark, A. Linden, K. C. Sturge and M. J. Zaworotko, *Organometallics, 7* (1988) 2571; (c) D. Astruc, *Top. Curr. Chem., 160* (1991) 47.
2 D. M. Braitsch, *J. Chem. Soc., Chem. Commun.,* (1974) 460.
3 R. E. Lehmann and J. K. Kochi, *J. Am. Chem. Soc., 113* (1991) 501.
4 R. S. Mulliken, *J. Am. Chem. Soc., 74* (1952) 811.
5 R. S. Mulliken and W. B. Person, *Molecular Complexes*, Wiley, New York, 1969.
6 C. W. Davis, *Ion Association*, Butterworth, London, 1962.
7 J. E. Gordon, *Organic Chemistry of Electrolyte Solutions*, Wiley, New York, 1975.
8 M. Swarcz, *Ions and Ion Pairs in Organic Reactions*, Vols. 1 and 2, Wiley, New York, 1972, 1974.
9 (a) E. M. Kosower, *J. Am. Chem. Soc., 80* (1958) 3253; (b) E. M. Kosower and J. A. Skorcz, *J. Am. Chem. Soc., 82* (1960) 2195; (c) E. M. Kosower and M. Mohammad, *J. Phys. Chem., 74* (1970) 1153.
10 T. M. Bockman and J. K. Kochi, *J. Am. Chem. Soc., 111* (1989) 4669.
11 T. M. Bockman, K. Y. Lee and J. K. Kochi, *J. Chem. Soc., Perkin Trans. 2,* (1992) 1581.
12 See T. A. Albright, J. K. Burdett and M. H. Whangbo, *Orbital Interactions in Chemistry*, Wiley, New York, 1985.
13 J. K. Kochi and T. M. Bockman, *Adv. Organomet. Chem., 33* (1991) 51.
14 E. O. Fischer and F. Röhrscheid, *Z. Naturforsch. B., 17* (1962) 483.
15 Compare: K. B. Yoon and J. K. Kochi, *J. Phys. Chem., 95* (1991) 1348.
16 T. W. Ebbesen and G. Ferraudi, *J. Phys. Chem., 87* (1983) 3717.
17 See also J. R. Barnett, A. S. Hopkins and A. Ledwith, *J. Chem. Soc., Perkin Trans. 2,* (1973) 80.
18 (a) H. G. Benesi and J. H. Hildebrand, *J. Am. Chem. Soc., 71* (1949) 2703; (b) W. B. Person, *J. Am. Chem. Soc., 67* (1965) 167.
19 Compare T. W. Ebbesen, L. E. Manring and K. S. Peters, *J. Am. Chem. Soc., 106* (1984) 7400.
20 Z. J. Karpinski and J. K. Kochi, *J. Organomet. Chem., 437* (1992) 211.

21 C. H. Wei and J. K. Kochi, unpublished results.
22 S. E. Anderson, Jr. and R. S. Drago, *J. Am. Chem. Soc., 92* (1970) 4244.
23 D. H. Busch and J. C. Bailar, Jr., *J. Am. Chem. Soc., 78* (1956) 1137; see also ref. 3.
24 W. Beck, W. Hieber and H. Tengler, *Chem. Ber., 94* (1961) 862.
25 K. Y. Lee and J. K. Kochi, *Inorg. Chem., 28* (1989) 567.
26 Compare D. J. Kuchynka and J. K. Kochi, *Inorg. Chem., 28* (1989) 855.
27 (a) I. Wender, H. W. Sternberg and M. Orchin, *J. Am. Chem. Soc., 74* (1952) 1216; (b) E. R. Tucchi and G.H. Gwynn, *J. Am. Chem. Soc., 86* (1964) 4838.
28 F. J. Weigert, *Comput. Chem., 11* (1987) 273.
29 C. W. Gear, *Numerical Value Problems in Ordinary Differential Equations*, Prentice-Hall, Englewood Cliffs, NJ, 1971.
30 M. Tilset and V. D. Parker, *J. Am. Chem. Soc., 111* (1989) 6711.
31 Z. J. Karpinski and J. K. Kochi, *Inorg. Chem., 31* (1992) 2762.
32 R. W. Wegman, R. J. Olsen, D. R. Gard, L. R. Faulkner and T. L. Brown, *J. Am. Chem. Soc., 103* (1981) 6089; see also ref. 26.
33 R. W. Wegman and T. L. Brown, *Inorg. Chem., 22* (1983) 183.
34 J. F. Helling and D. M. Braitsch, *J. Am. Chem. Soc., 92* (1970) 7207.
35 S. Trofimenko, E. L. Little and H. F. Mower, *J. Org. Chem., 27* (1962) 2795.
36 C. H. Wei, T. M. Bockman and J. K. Kochi, *J. Organomet. Chem., 428* (1992) 85.
37 Atlantic Microlab, Atlanta, GA.
38 Project Seraphim, 1101 University Ave, Madison, WI 53706, USA.
39 See also A. Vogler and H. Kunkely, *Organometallics, 7* (1988) 1449.